Available online at www.sciencedirect.com
ScienceDirect
Journal of Computational Physics 223 (2007) 469–488
JOURNAL OF COMPUTATIONAL PHYSICS
www.elsevier.com/locate/jcp

An optimal perfectly matched layer with unbounded absorbing function for time-harmonic acoustic scattering problems

A. Bermúdez [a,*], L. Hervella-Nieto [b], A. Prieto [a], R. Rodríguez [c]

[a] *Departamento de Matemática Aplicada, Universidade de Santiago de Compostela, 15706 Santiago de Compostela, Spain*
[b] *Departamento de Matemáticas, Universidade da Coruña, 15707 A Coruña, Spain*
[c] *GI²MA, Departamento de Ingeniería Matemática, Universidad de Concepción, Casilla 160-C, Concepción, Chile*

Received 29 March 2006; received in revised form 1 August 2006; accepted 20 September 2006
Available online 9 November 2006

Abstract

We introduce an optimal bounded perfectly matched layer (PML) technique by choosing a particular absorbing function with unbounded integral. With this choice, spurious reflections are avoided, even though the thickness of the layer is finite. We show that such choice is easy to implement in a finite element method and overcomes the dependency of parameters for the discrete problem. Finally, its efficiency and accuracy are illustrated with some numerical tests.

Keywords: Perfectly matched layer; Time-harmonic scattering; Helmholtz equation; Finite element method

1. Introduction

The first problem to be tackled for the numerical solution of any scattering problem in an unbounded domain is to truncate the computational domain without perturbing too much the solution of the original problem. In an ideal framework, the method should satisfy, at least, three properties: efficiency, easiness of implementation, and robustness.

Several numerical techniques have been developed with this purpose: boundary element methods, infinite element methods, Dirichlet-to-Neumann operators based on truncating Fourier expansions, absorbing boundary conditions, etc. The potential advantages of each of them have been widely studied in the literature (see, for instance, [2,16,24,29], and [19] for a classical review on this subject).

We focus our attention on the last mentioned technique: local absorbing boundary conditions (ABCs) can be used to preserve the computational efficiency of the numerical method. Those of Bayliss and Turkel [5],

* Corresponding author. Tel.: +34 981563100/13192; fax: +34 981597054.
E-mail addresses: mabermud@usc.es (A. Bermúdez), luisher@udc.es (L. Hervella-Nieto), maprieto@usc.es (A. Prieto), rodolfo@ing-mat.udec.cl (R. Rodríguez).

0021-9991/$ - see front matter
doi:10.1016/j.jcp.2006.09.018

Engquist and Majda [17], and Feng [18] are among the most widely used. However, in spite of the simple implementation of lowest order ABCs, good accuracy is only achieved for higher order ones [31], because these conditions are not fully non-reflecting on the truncated boundary of the computational domain. As a consequence, high accuracy using ABCs leads to a substantial computational cost and increases the difficulty of implementation. Recently, a promising way has been open: high order ABCs not involving high derivatives (see [20,25]).

An alternative approach to deal with the truncation of unbounded domains is the so-called *perfectly matched layer* (PML) method, which was introduced by Berenger [8–10]. It is based on simulating an absorbing layer of anisotropic damping material surrounding the domain of interest, like a thin sponge which absorbs the scattered field radiated to the exterior of this domain. This method is known as 'perfectly matched' because the interface between the physical domain and the absorbing layer does not produce spurious reflections inside the domain of interest.

This method has been applied to different problems. It was initially settled for Maxwell's equations in electromagnetism [7,8] and subsequently used for the scalar Helmholtz equation [21,30,33], advective acoustics [1,6,23], shallow water waves [28], elasticity [4,15], poroelastic media [34], and other hyperbolic problems (see for instance [27] among many other papers). We focus our attention on wave propagation time-harmonic scattering problems in linear acoustics, i.e., on the scalar Helmholtz equation.

In practice, since the PML has to be truncated at a finite distance of the domain of interest, its external boundary produces artificial reflections. Theoretically, these reflections are of minor importance because of the exponential decay of the acoustic waves inside the PML. In fact, for Helmholtz-type scattering problems, Lassas and Somersalo [26] proved, using boundary integral equation techniques, that the approximate solution obtained by the PML method converges exponentially to the exact solution in the computational domain as the thickness of the layer goes to infinity. This result was generalized by Hohage et al. [22] using techniques based on the pole condition. Similarly, Bécache et al. [6] proved an analogous result for the convected Helmholtz equation.

Once the problem is discretized, the approximation error typically becomes larger. Increasing the thickness of the PML may be a remedy, but not always available because of computational cost. An alternative usual choice to achieve low error levels is to take larger values for the absorption coefficients in the layer. However, Collino and Monk [14] showed that this methodology may produce an increasing error in the discretized problem. Consequently, an optimization problem arises: given a data set and a mesh, to choose an optimal absorbing function (i.e., a variable absorption coefficient) to minimize the error. In this framework, Asvadurov et al. [3] proposed a pure imaginary stretching to optimize the error of the PML method. They recovered exponential error estimates using finite-difference grid optimization. However, to the best of the authors' knowledge, the optimization problem is still open in that there is no optimal criterion to choose the absorbing function independently of data and meshes.

We have proposed in [11] an alternative procedure to avoid this drawback: to use an absorbing function with unbounded integral on the PML. We have shown in that reference that this leads to a theoretically exact bounded PML. More precisely, this kind of absorbing functions on a circular annular layer allows recovering of the exact solution of the time-harmonic scattering problem in the domain of interest, up to discretization errors, even though the thickness of the layer is finite.

In this paper, we consider Cartesian perfectly matched layers. We report numerical evidence that allows us to choose a particularly convenient non-integrable absorbing function. This function only depends on the sound speed of the fluid. We show that this choice leads to a robust PML method, easy to implement in a finite element code. We assess the efficiency of our choice by comparing it with classical bounded absorbing functions in test problems. We also report the numerical results obtained in some realistic examples.

The outline of this paper is as follows. In Section 2 we consider a simple problem: the propagation of plane waves with oblique incidence in a two-dimensional unbounded domain. We show that a PML method based on a non-integrable absorbing function allows recovering the exact solution in the domain of interest. In Section 3 we recall the classical two-dimensional scattering problem with Cartesian perfectly matched layers. In Section 4 we describe a finite element method to solve this problem. We show that for the resulting finite element problem to be well posed, it is necessary to impose further constraints on the absorbing function. In Section 5 we report the results of some numerical tests which allow us to choose the most convenient

non-integrable absorbing function. In Section 6 we show the advantages of our choice as compared with a classical PML based on a quadratic absorbing function. In Section 7, we report the numerical results obtained with our PML technique applied to some realistic wave propagation problems. Finally, in Appendix A, we show how the element matrices can be computed either by explicit integration or by means of quadrature rules.

2. Plane acoustic waves with oblique incidence

First, we consider a simple problem which will provide valuable information for the design of an efficient PML method: the propagation of two-dimensional acoustic plane waves with oblique incidence.

Consider the following time-harmonic problem posed in the right-half space:

$$\begin{cases} \Delta p + k^2 p = 0, \quad x > 0, \\ p(0,y) = \mathrm{e}^{\mathrm{i}k_y y}, \\ \lim\limits_{x\to+\infty} \left(\frac{\partial p}{\partial x} - \mathrm{i}k_x p\right) = 0, \end{cases} \tag{2.1}$$

where the unknown p is the amplitude of the pressure wave, $k = \omega/c$ is the wave number, with ω being the angular frequency of the waves and c the sound speed of the fluid. Moreover, $k_x = k\cos\theta$ and $k_y = k\sin\theta$, with θ being the incidence angle. The solution of this problem is the plane wave

$$p(x,y) = \mathrm{e}^{\mathrm{i}(k_x x + k_y y)}.$$

We introduce a PML in the vertical strip $a < x < a^*$, to truncate the unbounded domain in the x-direction (see Fig. 1). The strip $0 < x < a$ is the so called 'physical domain', where we are interested in computing the solution of problem (2.1).

We consider a variable absorption coefficient σ in the PML. This coefficient is allowed to be a function of the variable x; constant, linear or quadratic 'absorbing functions' are the typical choices (see, for instance, [6,8,13]). In our case, we will allow for any arbitrary non-negative absorbing function.

The deduction of the PML equations is nowadays well known (see, for instance, Section 3.3.4 in [24]). In our case, the amplitudes of the pressure waves in the physical domain, p_{F}, and in the PML, p_{A}, are the solution of the following equations:

$$\begin{cases} \Delta p_{\mathrm{F}} + k^2 p_{\mathrm{F}} = 0, \quad 0 < x < a, \\ \frac{1}{\gamma}\frac{\partial}{\partial x}\left(\frac{1}{\gamma}\frac{\partial p_{\mathrm{A}}}{\partial x}\right) + \frac{\partial^2 p_{\mathrm{A}}}{\partial y^2} + k^2 p_{\mathrm{A}} = 0, \quad a < x < a^*, \\ p_{\mathrm{F}}(0,y) = \mathrm{e}^{\mathrm{i}k_y y}, \\ p_{\mathrm{F}}(a,y) = p_{\mathrm{A}}(a,y), \\ \frac{\partial p_{\mathrm{F}}}{\partial x}(a,y) = \frac{1}{\gamma(a)}\frac{\partial p_{\mathrm{A}}}{\partial x}(a,y), \\ p_{\mathrm{A}}(a^*,y) = 0, \end{cases}$$

with

$$\gamma(x) = \begin{cases} 1, & \text{if } 0 < x < a, \\ 1 + \frac{\mathrm{i}}{\omega}\sigma(x), & \text{if } a \leqslant x < a^*. \end{cases}$$

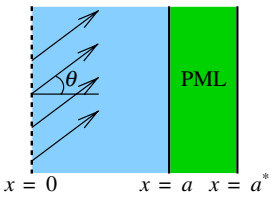

Fig. 1. PML in the x-direction for plane waves with oblique incidence.

To solve this problem, we follow [12] and introduce the complex change of variable

$$\hat{x}(x) = \int_0^x \gamma(s)\,\mathrm{d}s = x + \frac{\mathrm{i}}{\omega}\int_a^x \sigma(s)\,\mathrm{d}s, \quad x \in [a, a^*). \tag{2.2}$$

Thus

$$\frac{\partial \hat{x}}{\partial x} = \gamma \quad \text{and} \quad \frac{\partial}{\partial \hat{x}} = \frac{1}{\gamma}\frac{\partial}{\partial x}.$$

Hence, if we denote $\hat{p}_{\mathrm{A}}(\hat{x}, y) = p_{\mathrm{A}}(x, y)$, then we have that

$$\frac{1}{\gamma}\frac{\partial}{\partial x}\left(\frac{1}{\gamma}\frac{p_{\mathrm{A}}}{\partial x}\right) + \frac{\partial^2 p_{\mathrm{A}}}{\partial y^2} + k^2 p_{\mathrm{A}} = 0 \quad \Longleftrightarrow \quad \frac{\partial^2 \hat{p}_{\mathrm{A}}}{\partial \hat{x}^2} + \frac{\partial^2 \hat{p}_{\mathrm{A}}}{\partial y^2} + k^2 \hat{p}_{\mathrm{A}} = 0.$$

Therefore, the solution of the PML problem can be written as superposition of plane waves:

$$\begin{cases} p_{\mathrm{F}}(x, y) = (I\mathrm{e}^{\mathrm{i}k_x x} + R_{\mathrm{F}}\mathrm{e}^{-\mathrm{i}k_x x})\mathrm{e}^{\mathrm{i}k_y y}, & x \in (0, a), \\ \hat{p}_{\mathrm{A}}(\hat{x}, y) = (T\mathrm{e}^{\mathrm{i}k_x \hat{x}} + R_{\mathrm{A}}\mathrm{e}^{-\mathrm{i}k_x \hat{x}})\mathrm{e}^{\mathrm{i}k_y y}, & x \in [a, a^*), \end{cases}$$

where I is the amplitude of the incident wave, T that of the wave transmitted to the PML, and R_{F} and R_{A} are the amplitudes of the reflected waves in the physical domain and in the absorbing layer, respectively.

By substituting (2.2) in the last equation, we can write the solution in the absorbing layer in the following equivalent form:

$$p_{\mathrm{A}}(x, y) = \left[T\mathrm{e}^{\mathrm{i}k_x x}\mathrm{e}^{-\frac{\cos\theta}{c}\int_a^x \sigma(s)\,\mathrm{d}s} + R_{\mathrm{A}}\mathrm{e}^{-\mathrm{i}k_x x}\mathrm{e}^{\frac{\cos\theta}{c}\int_a^x \sigma(s)\,\mathrm{d}s}\right]\mathrm{e}^{\mathrm{i}k_y y}.$$

Next, from the boundary condition at $x = 0$, we obtain

$$I = 1 - R_{\mathrm{F}}.$$

On the other hand, from the transmission conditions at $x = a$, we have

$$R_{\mathrm{F}} = R_{\mathrm{A}} \quad \text{and} \quad I = T.$$

Notice that the latter implies that no spurious reflections arise at $x = a$ (which is the main feature of the PML techniques); the terms involving R_{F} and R_{A} arise as a consequence of the waves reflected at $x = a^*$. Finally, the homogeneous Dirichlet boundary condition at $x = a^*$ yields

$$R_{\mathrm{A}} = \frac{\mathrm{e}^{2\mathrm{i}k_x a^*}}{\mathrm{e}^{2\mathrm{i}k_x a^*} - \mathrm{e}^{\frac{2\cos\theta}{c}\int_a^{a^*} \sigma(s)\,\mathrm{d}s}}. \tag{2.3}$$

Summarizing, we have obtained the following analytical expression for the solution of the PML problem above:

$$\begin{cases} p_{\mathrm{F}}(x, y) = [(1 - R_{\mathrm{A}})\mathrm{e}^{\mathrm{i}k_x x} + R_{\mathrm{A}}\mathrm{e}^{-\mathrm{i}k_x x}]\mathrm{e}^{\mathrm{i}k_y y}, & x \in (0, a), \\ p_{\mathrm{A}}(x, y) = \left[(1 - R_{\mathrm{A}})\mathrm{e}^{\mathrm{i}k_x x}\mathrm{e}^{-\frac{\cos\theta}{c}\int_a^x \sigma(s)\,\mathrm{d}s} + R_{\mathrm{A}}\mathrm{e}^{-\mathrm{i}k_x x}\mathrm{e}^{\frac{\cos\theta}{c}\int_a^x \sigma(s)\,\mathrm{d}s}\right]\mathrm{e}^{\mathrm{i}k_y y}, & x \in [a, a^*). \end{cases}$$

The expression (2.3) for R_{A} shows that the larger the integral $\int_a^{a^*} \sigma(s)\,\mathrm{d}s$, the closer R_{A} to zero and, consequently, the closer p_{F} to the solution p of problem (2.1) in the physical domain. Indeed, straightforward computations lead to

$$\int_0^a |p(x, y) - p_{\mathrm{F}}(x, y)|^2\,\mathrm{d}x = |R_{\mathrm{A}}|^2\,\frac{2k_x a - \sin(2k_x a)}{k_x}.$$

Classical PML techniques rely on taking a bounded absorbing function σ, such that its integral be sufficiently large. We propose instead to use an unbounded σ such that

$$\int_a^{a^*} \sigma(s)\,\mathrm{d}s = +\infty.$$

In this case, $R_A = 0$ and, consequently, the resulting p_F will coincide exactly with the solution p of problem (2.1) in the physical domain.

3. The time-harmonic acoustic scattering problem

We deal with the time-harmonic acoustic scattering problem in an unbounded exterior 2D domain. Let Ω be a bounded domain of $\mathbb{R}^2$ occupied by an obstacle to the propagation of acoustic waves; we assume the obstacle has a totally reflecting boundary Γ, with outer normal unit vector $\mathbf{n}$ (see Fig. 2). Our goal is to solve the following exterior Helmholtz problem with Neumann boundary data:

$$\begin{cases} \Delta p + k^2 p = 0 \quad \text{in } \mathbb{R}^2 \setminus \Omega, \\ \frac{\partial p}{\partial \mathbf{n}} = g \quad \text{on } \Gamma, \\ \lim_{r\to\infty} \sqrt{r}\left(\frac{\partial p}{\partial r} - \mathrm{i}kp\right) = 0. \end{cases} \tag{3.1}$$

Once more, p is the unknown amplitude of the pressure wave and $k = \omega/c$ is the wave number, with ω being the angular frequency of the waves and c the sound speed of the fluid in the exterior domain.

We introduce perfectly matched layers (PML) on the x and y directions to truncate the unbounded domain, as shown in Fig. 3. The inner rectangle contains the obstacle Ω as well as the physical domain Ω_F, i.e., the subdomain occupied by the fluid surrounding the obstacle where we are interested in computing the solution of (3.1).

We use the notation introduced in Fig. 3. In particular, Ω_A denotes the absorbing layer, Γ_I the interface between the physical domain and the layer, Γ_D the outer boundary, and $\boldsymbol{\nu} = (\nu_x, \nu_y)$ the unit normal vector to Γ_I outward to Ω_F.

We consider now variable absorption coefficients in the PML, σ_x and σ_y, acting on the vertical and horizontal layers, respectively; moreover, both absorption coefficients act in the corner layers. These coefficients, σ_x and σ_y, are allowed to be functions of x and y, respectively. Although constant, linear or quadratic functions are the typical choices, we proceed as in the previous section, and allow for arbitrary non-negative absorbing functions $\sigma_x(|x|)$ and $\sigma_y(|y|)$.

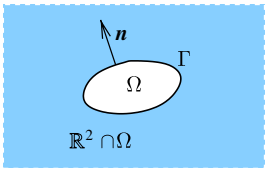

Fig. 2. Two-dimensional unbounded domain.

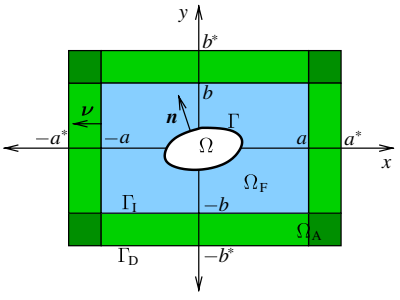

Fig. 3. Cartesian PML on a two-dimensional domain.

The amplitudes of the pressure waves in the physical domain, p_F, and in the PML, p_A, are the solution of the following equations (see, for instance, [13]):

$$\begin{cases} \Delta p_F + k^2 p_F = 0 \quad \text{in } \Omega_F, \\ \frac{1}{\gamma_x}\frac{\partial}{\partial x}\left(\frac{1}{\gamma_x}\frac{\partial p_A}{\partial x}\right) + \frac{1}{\gamma_y}\frac{\partial}{\partial y}\left(\frac{1}{\gamma_y}\frac{\partial p_A}{\partial y}\right) + k^2 p_A = 0 \quad \text{in } \Omega_A, \\ \frac{\partial p_F}{\partial \mathbf{n}} = g \quad \text{on } \Gamma, \\ p_F = p_A \quad \text{on } \Gamma_I, \\ \frac{\partial p_F}{\partial v_x} + \frac{\partial p_F}{\partial v_y} = \frac{1}{\gamma_x}\frac{\partial p_A}{\partial v_x} + \frac{1}{\gamma_y}\frac{\partial p_A}{\partial v_y} \quad \text{on } \Gamma_I, \\ p_A = 0 \quad \text{on } \Gamma_D, \end{cases} \tag{3.2}$$

where

$$\gamma_x(x) = \begin{cases} 1, & \text{if } |x| < a, \\ 1 + \frac{i}{\omega}\sigma_x(|x|), & \text{if } a \leqslant |x| < a^*, \end{cases}$$

and

$$\gamma_y(y) = \begin{cases} 1, & \text{if } |y| < b, \\ 1 + \frac{i}{\omega}\sigma_y(|y|), & \text{if } b \leqslant |y| < b^*. \end{cases}$$

The main goal of this paper is to determine how to choose the absorbing functions σ_x and σ_y, so that p_F be an approximation as close as possible to the solution p of problem (3.1) in the physical domain. According to the results of the previous section, the natural candidates are unbounded functions σ_x and σ_y such that

$$\int_a^{a^*} \sigma_x(s)\,ds = +\infty \quad \text{and} \quad \int_b^{b^*} \sigma_y(s)\,ds = +\infty.$$

4. Finite element discretization

In this section we describe a finite element method for the numerical solution of (3.2) and show that the resulting discrete problem is well posed only for certain unbounded absorbing functions. This will lead to additional constraints on σ_x and σ_y.

We consider a partition in triangles of the physical domain Ω_F and a partition in rectangles of the absorbing layer Ω_A, matching on the common interface Γ_I as shown in Fig. 4. As usual, h denotes the mesh-size.

The reason why we use such hybrid meshes is that triangles are more adequate to fit the boundary of the obstacle, whereas rectangles will allow us to compute explicitly the integrals involving the absorbing function that will appear in the elements in the layer. This is not strictly necessary, since these integrals can also be efficiently computed by means of standard quadrature rules as shown in Appendix A. However, in this paper, we will mainly consider exact integration to be able to assess the accuracy of the proposed PML independently of quadrature errors.

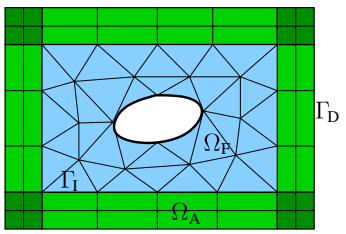

Fig. 4. Hybrid mesh on PML and physical domain.

We will compute approximations p_{F}^h and p_{A}^h of the pressure amplitude in the physical domain and in the absorbing layer, respectively, by using linear triangular finite elements for the former and bilinear rectangular finite elements for the latter. The degrees of freedom defining the finite element solution are the values of p_{F}^h and p_{A}^h at the vertices of the elements. Notice that because of the transmission condition $p_{\mathrm{F}} = p_{\mathrm{A}}$ on Γ_{I}, the values of p_{F}^h and p_{A}^h must coincide at the vertices on the interface.

Moreover, we impose the Dirichlet boundary condition $p_{\mathrm{A}}^h = 0$ on Γ_{D} on the finite element solution. Hence, p_{A}^h does not have degrees of freedom on the outer boundary. This fact will be essential for the resulting discrete problem to be well posed.

Standard arguments in this finite element framework lead to the following discrete problem from the weak formulation of problem (3.2):

$$\int_{\Omega_{\mathrm{F}}} \nabla p_{\mathrm{F}}^h \cdot \nabla \bar{q}^h \,\mathrm{d}x\,\mathrm{d}y - \int_{\Omega_{\mathrm{F}}} k^2 p_{\mathrm{F}}^h \bar{q}^h \,\mathrm{d}x\,\mathrm{d}y + \int_{\Omega_{\mathrm{A}}} \frac{\gamma_y}{\gamma_x} \frac{\partial p_{\mathrm{A}}^h}{\partial x} \frac{\partial \bar{q}^h}{\partial x} \,\mathrm{d}x\,\mathrm{d}y + \int_{\Omega_{\mathrm{A}}} \frac{\gamma_x}{\gamma_y} \frac{\partial p_{\mathrm{A}}^h}{\partial y} \frac{\partial \bar{q}^h}{\partial y} \,\mathrm{d}x\,\mathrm{d}y - \int_{\Omega_{\mathrm{A}}} k^2 \gamma_x \gamma_y p_{\mathrm{A}}^h \bar{q}^h \,\mathrm{d}x\,\mathrm{d}y = \int_{\Gamma} g \bar{q}^h \,\mathrm{d}s,$$

for all functions q^h, continuous in $\Omega_{\mathrm{F}} \cup \Omega_{\mathrm{A}}$, piecewise linear in Ω_{F}, piecewise bilinear in Ω_{A}, and vanishing on Γ_{D}.

Once the discrete problem is written in matrix form, it yields a system of linear equations whose unknowns are the nodal values of p_{F}^h and p_{A}^h. The entries of the system matrix are computed by assembling the element matrices; in particular, the following ones involve the unbounded absorbing functions:

$$\int_K \frac{\gamma_y}{\gamma_x} \frac{\partial N_i}{\partial x} \frac{\partial N_j}{\partial x} \,\mathrm{d}x\,\mathrm{d}y, \quad \int_K \frac{\gamma_x}{\gamma_y} \frac{\partial N_i}{\partial y} \frac{\partial N_j}{\partial y} \,\mathrm{d}x\,\mathrm{d}y, \quad \text{and} \quad \int_K k^2 \gamma_x \gamma_y N_i N_j \,\mathrm{d}x\,\mathrm{d}y, \tag{4.1}$$

with K being a rectangular element in Ω_{A} and $\{N_i\}$ the nodal finite element basis.

For the discrete problem to be well posed, it is necessary that all the integrals above be finite, what is not trivial since they involve singular functions whenever K is a rectangle with an edge lying on the outer boundary Γ_{D}.

For instance, consider the element K shown in Fig. 5 (the forthcoming arguments and conclusions hold also true for all other elements with edges lying on Γ_{D}). Notice that, since p_{A}^h vanishes at the vertices on Γ_{D}, we only need to compute in this element the integrals (4.1) for the nodal functions N_1 and N_2 associated with the vertices denoted by P_1 and P_2, respectively.

These functions are given by

$$N_1(x,y) = \frac{(x-a^*)(y-b_2)}{h_x h_y}, \quad N_2(x,y) = -\frac{(x-a^*)(y-b_1)}{h_x h_y},$$

and their partial derivatives by

$$\frac{\partial N_1}{\partial x}(x,y) = \frac{y-b_2}{h_x h_y}, \quad \frac{\partial N_2}{\partial x}(x,y) = -\frac{y-b_1}{h_x h_y},$$
$$\frac{\partial N_1}{\partial y}(x,y) = \frac{x-a^*}{h_x h_y}, \quad \frac{\partial N_2}{\partial y}(x,y) = -\frac{x-a^*}{h_x h_y}.$$

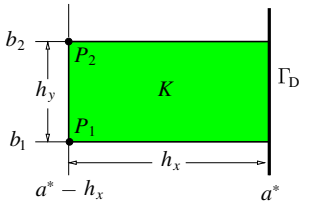

Fig. 5. Finite element with an edge lying on Γ_{D}.

Therefore, the integrals in (4.1) can be written as follows:

$$\int_K \frac{\gamma_y}{\gamma_x}\frac{\partial N_i}{\partial x}\frac{\partial N_j}{\partial x}\,\mathrm{d}x\,\mathrm{d}y = \pm\frac{1}{h_x^2h_y^2}\int_{b_1}^{b_2}\gamma_y(y)(y-b_j)(y-b_i)\,\mathrm{d}y\int_{a^*-h_x}^{a^*}\frac{\mathrm{d}x}{\gamma_x(x)}, \tag{4.2}$$

$$\int_K \frac{\gamma_x}{\gamma_y}\frac{\partial N_i}{\partial y}\frac{\partial N_j}{\partial y}\,\mathrm{d}x\mathrm{d}y = \pm\frac{1}{h_x^2h_y^2}\int_{b_1}^{b_2}\frac{\mathrm{d}y}{\gamma_y(y)}\int_{a^*-h_x}^{a^*}\gamma_x(x)(x-a^*)^2\,\mathrm{d}x, \tag{4.3}$$

$$\int_K \gamma_x\gamma_y N_iN_j\,\mathrm{d}x\,\mathrm{d}y = -\frac{1}{h_x^2h_y^2}\int_{b_1}^{b_2}\gamma_y(y)(y-b_j)(y-b_i)\,\mathrm{d}y\int_{a^*-h_x}^{a^*}\gamma_x(x)(x-a^*)^2\,\mathrm{d}x. \tag{4.4}$$

We assume singularities of power type for the absorbing functions:

$$\sigma_x(x) = \mathcal{O}((a^*-x)^{-\alpha}) \text{ as } \quad x\to a^*, \quad \sigma_y(y) = \mathcal{O}((b^*-y)^{-\alpha}) \quad y\to b^*. \tag{4.5}$$

Notice that the constraint that σ_x and σ_y have unbounded integrals holds true if and only if $\alpha \geqslant 1$.

From the definitions of γ_x and γ_y we have that $\gamma_x(x) = \mathcal{O}((a^*-|x|)^{-\alpha})$ and $\gamma_y(y) = \mathcal{O}((b^*-|y|)^{-\alpha})$. Moreover, $|\gamma_x|\geqslant 1$ and $|\gamma_y|\geqslant 1$ and, hence, the integrals of $1/\gamma_x(x)$ and $1/\gamma_y(y)$ are always finite.

For an element K as that in Fig. 5, γ_y is bounded in the interval $[b_1,b_2]$ and, consequently, the integrals involving $\gamma_y(y)$ are also finite. Finally, for the integral involving $\gamma_x(x)$ we have

$$\int_{a^*-h}^{a^*}\gamma_x(x)(x-a^*)^2\,\mathrm{d}x = \int_{a^*-h}^{a^*}\mathcal{O}((a^*-x)^{2-\alpha})\,\mathrm{d}x<\infty \quad \Longleftrightarrow \quad \alpha<3.$$

As a consequence of this analysis, we will restrict our choice of σ_x and σ_y as in (4.5) to exponents α satisfying $1\leqslant\alpha<3$.

5. Determination of the absorbing function

In this section we report the numerical experimentation performed to determine the most convenient unbounded absorbing functions. With this purpose, we have applied our PML method with different σ_x and σ_y to a scattering problem with known analytical solution and compared the accuracy of the numerical results.

Consider problem (3.1) where the obstacle Ω is the unit circle centered at the origin. Given any inner point (x_0,y_0) of this circle, it is well known that the function

$$p(x,y) = \frac{\mathrm{i}}{4}H_0^{(1)}\left(k\sqrt{(x-x_0)^2+(y-y_0)^2}\right)$$

satisfies the first and third equations of (3.1). Therefore, if we take $g=\partial p/\partial\mathbf{n}$, then p is the unique solution of this problem.

In our experiments we have taken $x_0 = 0.5$ m, $y_0 = 0$, and $k=\omega/c$, with $c = 340$ m/s and different values of the frequency ω. For our computational domain we have taken $a=b=2.0$ m and $a^*=b^*=2.25$ m (see Fig. 6).

We have used uniform refinements of the mesh shown in Fig. 6; the number N of elements through the thickness of the PML is used to label each mesh.

To measure the accuracy we have computed the relative error in the L^2-norm in Ω_{F}:

$$\text{Error} = \frac{\left(\int_{\Omega_{\mathrm{F}}}|p_{\mathrm{F}}^h-p|^2\,\mathrm{d}x\,\mathrm{d}y\right)^{1/2}}{\left(\int_{\Omega_{\mathrm{F}}}|p|^2\,\mathrm{d}x\,\mathrm{d}y\right)^{1/2}}, \tag{5.1}$$

where p_{F}^h is the numerical solution in the physical domain and p the analytical solution.

According to the results of the previous section, it is enough to restrict the analysis to absorbing functions satisfying (4.5) with $1\leqslant\alpha<3$. We have considered the integer powers: $\alpha=1$ and $\alpha=2$. In particular, we have tested functions of the following type, where β is a free parameter to be fitted:

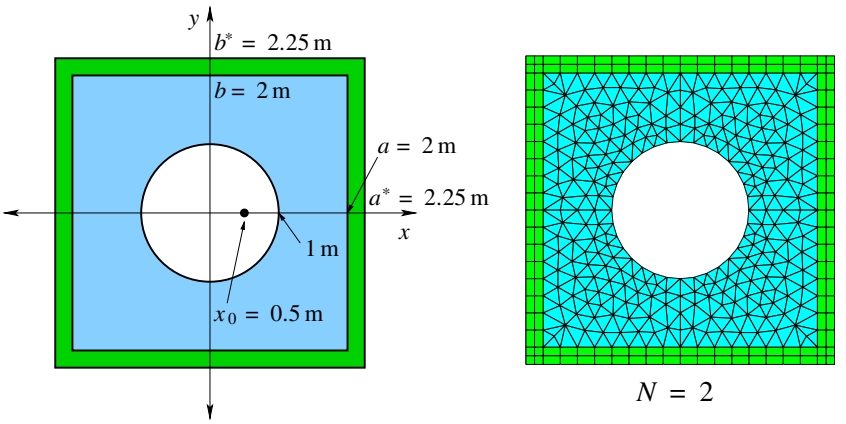

Fig. 6. Domains and mesh in the scattering problem.

- **A.** $\sigma_x(x) = \dfrac{\beta}{a^* - x}, \quad \sigma_y(y) = \dfrac{\beta}{b^* - y};$
- **B.** $\sigma_x(x) = \dfrac{\beta}{(a^* - x)^2}, \quad \sigma_y(y) = \dfrac{\beta}{(b^* - y)^2}.$

Notice that, in both cases, $\sigma_x(a) \neq 0$ and $\sigma_y(b) \neq 0$. Hence, the corresponding coefficients γ_x and γ_y will be discontinuous. To avoid eventual side effects of these discontinuities in the coupling conditions on Γ_I, we have also considered functions of the following type, which yield continuous γ_x and γ_y:

- **C.** $\sigma_x(x) = \dfrac{\beta}{a^* - x} - \dfrac{\beta}{a^* - a}, \quad \sigma_y(y) = \dfrac{\beta}{b^* - y} - \dfrac{\beta}{b^* - b},$
- **D.** $\sigma_x(x) = \dfrac{\beta}{(a^* - x)^2} - \dfrac{\beta}{(a^* - a)^2}, \quad \sigma_y(y) = \dfrac{\beta}{(b^* - y)^2} - \dfrac{\beta}{(b^* - b)^2}.$

In each case, we have fitted the parameter β so as to minimize the error. Figs. 7–12 show the results obtained with each type of absorbing functions and a range of values of β. We have used three meshes with refinement levels $N = 2$, 4, and 8, which have 464, 1720, and 6768 vertices, respectively. We report the results obtained with two frequencies: $\omega = 250$ rad/s and $\omega = 750$ rad/s.

We report in Table 1 the minimal relative errors and the optimal values of β determined for each type of absorbing function and each of the three meshes. It can be clearly seen from Table 1 that the smallest errors are always attained for a function of type **A** with the parameter $\beta \approx c$. To allow for comparison, we also include in Table 1 the errors for this choice; namely,

$$\sigma_x(x) = \frac{c}{a^* - x}, \quad \sigma_y(y) = \frac{c}{b^* - y}. \tag{5.2}$$

Let us remark that, for each mesh, the CPU time needed to solve the problem is essentially the same for the four types of absorbing functions. The condition numbers of the system matrices remain basically of the same order of magnitude for all the choices, too.

As a definite conclusion of this experimentation, we propose to use the absorbing functions (5.2). Notice that an additional advantage of this proposal is that the resulting PML method does not need of any parameter to be determined.

To assess the order of convergence of the proposed numerical method, we show in Fig. 13 the error curves (log–log plots of errors versus mesh-size) for $\omega = 250$ rad/s and $\omega = 750$ rad/s. It can be seen from this figure that an order of convergence $\mathcal{O}(h^2)$ is achieved. Let us recall that this is the optimal order for the used finite elements in L^2-norm.

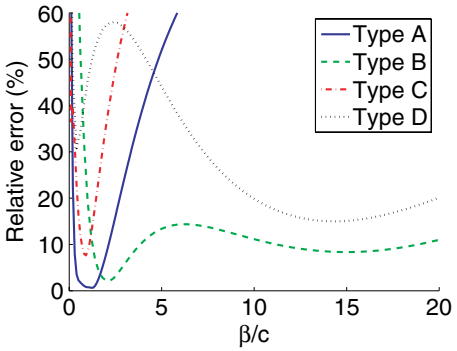

Fig. 7. Relative errors for PML with different unbounded absorbing functions. Mesh: $N = 2$; $\omega = 250$ rad/s.

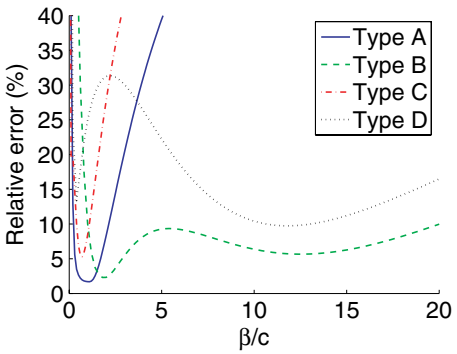

Fig. 8. Relative errors for PML with different unbounded absorbing functions. Mesh: $N = 2$; $\omega = 750$ rad/s.

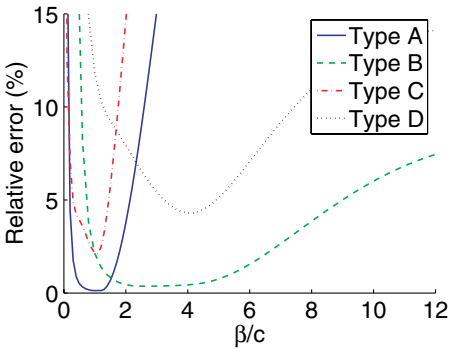

Fig. 9. Relative errors for PML with different unbounded absorbing functions. Mesh: $N = 4$; $\omega = 250$ rad/s.

To end this section, we show in Fig. 14 the real and imaginary parts of the solution computed with the proposed PML method for the mesh corresponding to $N = 8$ and $\omega = 750$ rad/s. The solution is plotted in the physical domain and in the PML.

6. Comparison with classical absorbing functions

The aim of this section is to compare the proposed unbounded absorbing function (5.2) with the most competitive classical choice: quadratic functions of the form

$$\sigma_x(x) = \sigma^*(x-a)^2 \quad \text{and} \quad \sigma_y(y) = \sigma^*(y-b)^2, \tag{6.1}$$

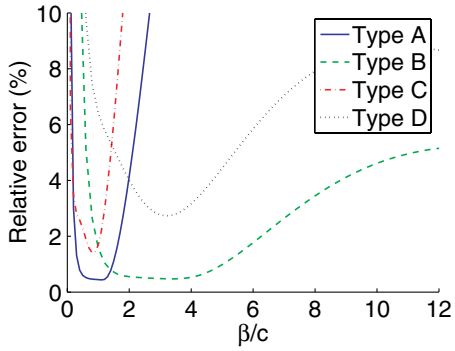

Fig. 10. Relative errors for PML with different unbounded absorbing functions. Mesh: $N = 4$; $\omega = 750$ rad/s.

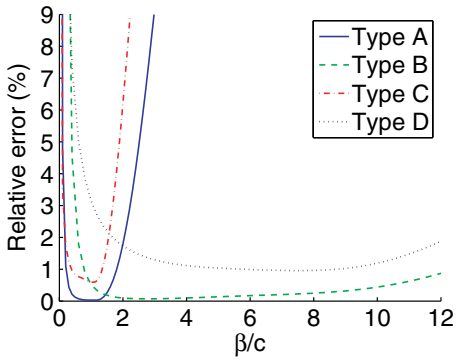

Fig. 11. Relative errors for PML with different unbounded absorbing functions. Mesh: $N = 8$; $\omega = 250$ rad/s.

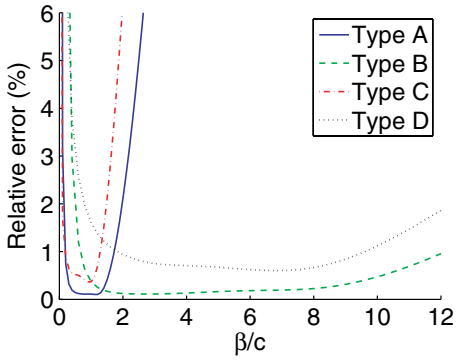

Fig. 12. Relative errors for PML with different unbounded absorbing functions. Mesh: $N = 8$; $\omega = 750$ rad/s.

where σ^* is a parameter to be determined. For the comparison we have used the same numerical test as in the previous section.

When these quadratic absorbing functions are used, the standard procedure to minimize the spurious reflections produced at the outer boundary of the PML consists of taking large values for σ^*. Notice that this agrees with the analysis in Section 2. However, larger values of σ^* lead to larger discretization errors. Therefore, σ^* cannot be chosen arbitrarily large because, otherwise, the discretization errors would be dominant, deteriorating the overall accuracy of the method.

Table 1
Minimal errors and optimal values of the parameter β for PML with different unbounded absorbing functions

Mesh	Type	$\omega = 250$ rad/s		$\omega = 750$ rad/s	
		β	Error (%)	β	Error (%)
$N = 2$	**A**	1.2 c	0.646	1.1 c	1.696
	B	2.2 c	2.160	1.8 c	2.305
	C	0.9 c	7.646	0.7 c	5.318
	D	14.4 c	14.995	11.8 c	9.739
	(5.2)	c	0.763	c	1.700
$N = 4$	**A**	1.0 c	0.131	1.1 c	0.437
	B	2.6 c	0.367	3.4 c	0.474
	C	1.1 c	2.113	0.8 c	1.411
	D	4.0 c	4.297	3.2 c	2.729
	(5.2)	c	0.131	c	0.447
$N = 8$	**A**	1.0 c	0.029	1.2 c	0.101
	B	2.8 c	0.070	2.6 c	0.111
	C	1.1 c	0.589	0.9 c	0.365
	D	7.6 c	0.957	6.8 c	0.602
	(5.2)	c	0.029	c	0.109

As shown in [14], for a given problem and a given mesh there is an optimal value of σ^* leading to minimal errors. Unfortunately, such optimal value depends strongly on the problem data as well as on the particular mesh. Thus, in practice, it is necessary to find in advance a reasonable value of σ^*. No theoretical procedure to tune this parameter is known to date. Some efforts have been done in [32], but the dependency of σ^* with respect to the mesh has not been avoided.

Let us emphasize that a benefit of our proposed PML strategy is that it does not need of any parameter to be fitted.

In Table 2, we compare the errors of the PML method with the unbounded absorbing functions (5.2) and with the quadratic absorbing functions (6.1). For the latter, we have used the optimal value of σ^*, which is also reported in Table 2. We also include in the table the condition number κ of the system matrix for each discrete problem.

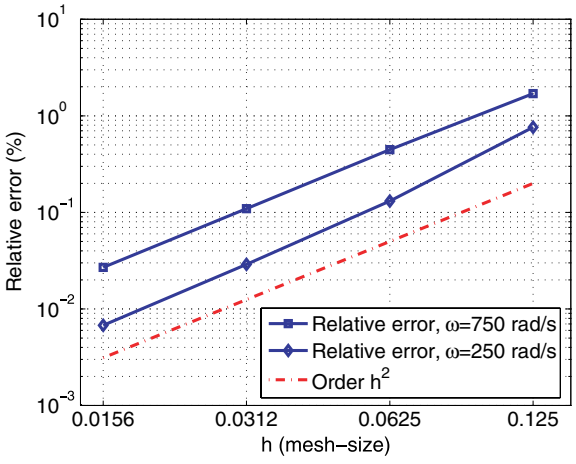

Fig. 13. Error curves of the PML method with absorbing functions (5.2).

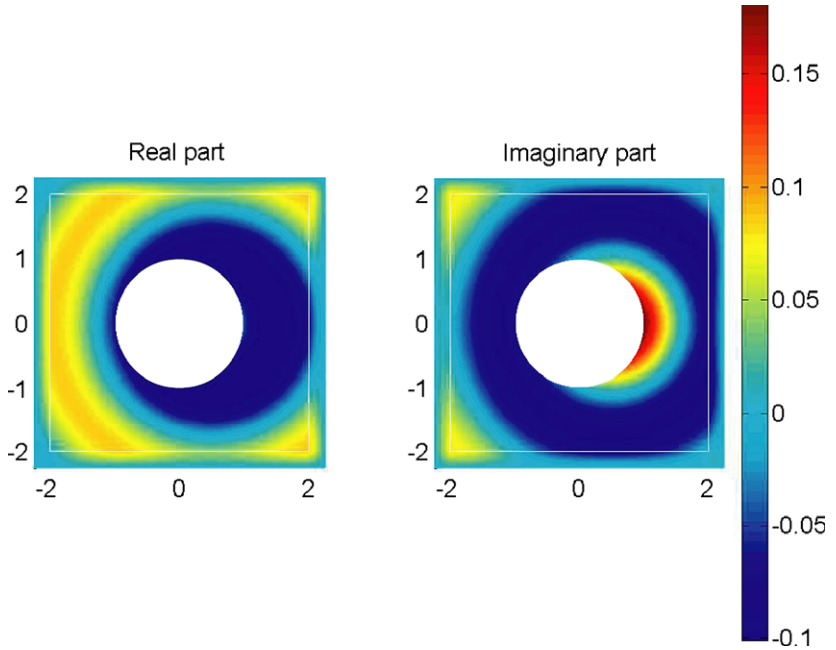

Fig. 14. Solution of the scattering problem computed by the PML method with absorbing functions (5.2). Mesh $N = 8$; $\omega = 750$ rad/s.

A significant advantage of the proposed unbounded absorbing functions (5.2) can be clearly appreciated from Table 2. This is particularly remarkable for lowest frequencies, but the errors with the quadratic absorbing functions are larger in all cases, even though the optimal value of σ^* has been used. On the other hand, in spite of the singular character of the unbounded functions, the condition numbers of the resulting system matrices are essentially of the same order as those of the quadratic functions.

On the other hand, Table 2 also shows that the optimal value of σ^* strongly depends on the problem data (the frequency ω in this case) and the mesh. The errors and the condition numbers would be significantly larger if any other value than the optimal σ^* were used. This can be appreciated from Figs. 15 and 16, where the relative error and the condition number are respectively plotted as functions of σ^*, for the mesh corresponding to $N = 4$ and $\omega = 750$ rad/s.

As a conclusion, the proposed PML method with unbounded absorbing function (5.2) clearly beats the classical choice of bounded absorbing functions. Moreover, it overcomes the problem of determining optimal parameters.

Table 2
Comparison of PML methods with unbounded and quadratic absorbing functions

ω (rad/s)	Mesh	Unbounded (5.2)		Quadratic (6.1)		
		Error (%)	κ	σ^*	Error (%)	κ
250	$N = 2$	0.763	6.7e + 02	22.28 c	11.644	4.7e + 02
	$N = 4$	0.131	5.1e + 03	29.57 c	3.675	5.0e + 03
	$N = 8$	0.029	4.1e + 04	38.37 c	1.134	4.6e + 04
750	$N = 2$	1.700	1.1e + 02	27.67 c	7.602	1.1e + 02
	$N = 4$	0.447	7.0e + 02	35.52 c	2.291	9.4e + 02
	$N = 8$	0.109	5.6e + 03	43.49 c	0.698	8.2e + 03
1250	$N = 2$	6.958	2.7e + 02	27.89 c	11.620	2.9e + 02
	$N = 4$	1.946	1.1e + 03	36.94 c	3.336	1.7e + 03
	$N = 8$	0.430	2.3e + 03	45.70 c	0.919	1.5e + 03

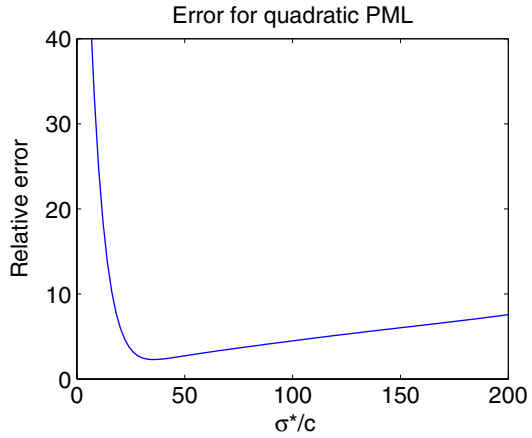

Fig. 15. Relative error for quadratic absorbing functions with varying σ^*. Mesh: $N = 4$; $\omega = 750$ rad/s.

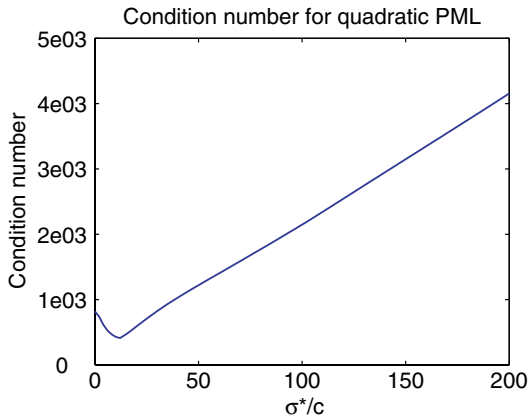

Fig. 16. Condition number for quadratic absorbing functions with varying σ^*. Mesh: $N = 4$; $\omega = 750$ rad/s.

7. Numerical tests

In this section, we report the results obtained by applying the proposed PML strategy based on the non-integrable absorbing function (5.2) to solve two 'real life' Helmholtz problems.

The first test is the scattering of an incident plane wave on the annular obstacle shown in Fig. 17. The wave number has been taken $k = 2\pi$ and the acoustic speed $c = 340$ m/s.

We have used our PML method on the two embedded square domains shown in Figs. 18 and 19. Therefore, we have been able to compare the numerical results as a mean of assessing the accuracy of the method, since an analytical solution of this problem is not available.

We have used uniform refinements of the meshes shown in Figs. 18 and 19, with 21160 triangles and 3328 rectangles for the smaller domain, and with 64680 triangles and 5888 rectangles for the larger.

In Figs. 20 and 21 we show the real and imaginary parts, respectively, of the computed solutions in both domains. It can be seen that both solutions are almost identical on the common part of the physical domains. Indeed, the relative difference in L^2-norm (which is defined analogously to (5.1)) is only 0.233%. Therefore, the solution computed in the smaller domain (and consequently with less computational effort) can be safely used.

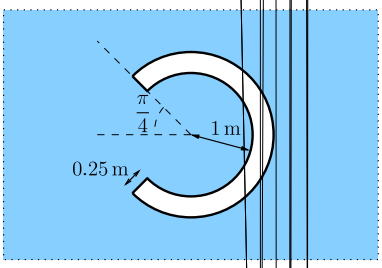

Fig. 17. Annular obstacle of the scattering problem.

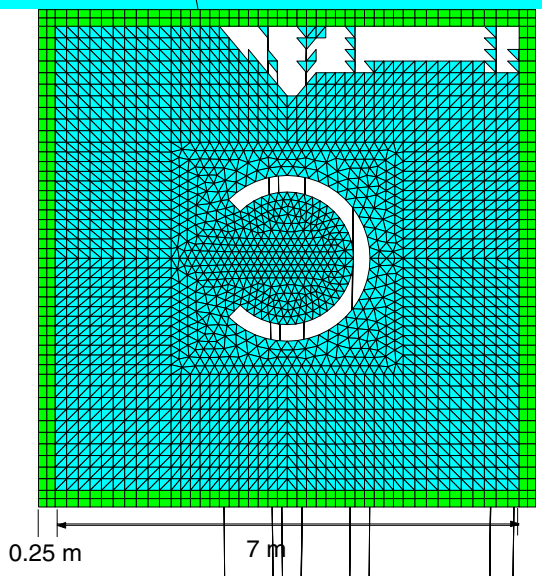

Fig. 19. Larger domain and coarse mesh for the scattering problem.

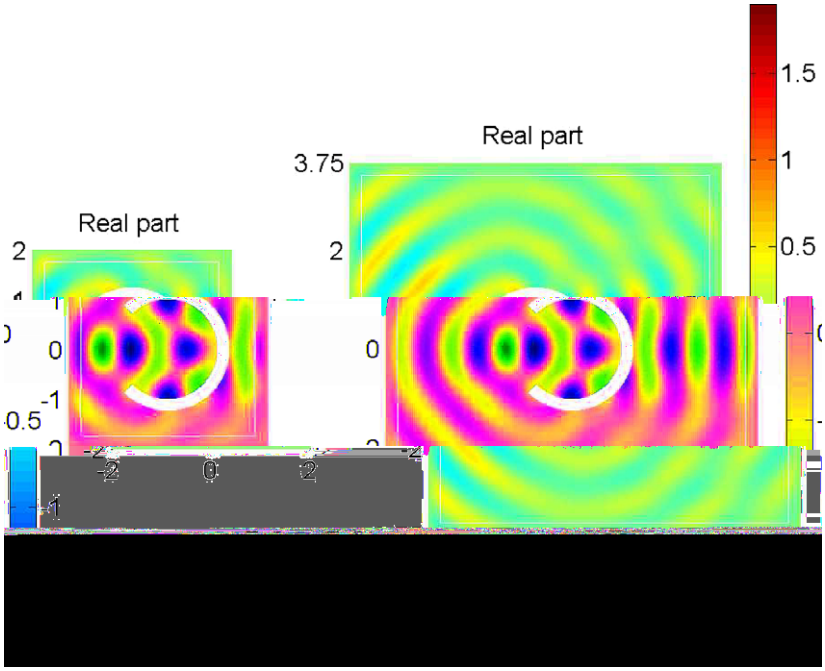

Fig. 20. Reflected wave field generated by an incident plane wave. Real part.

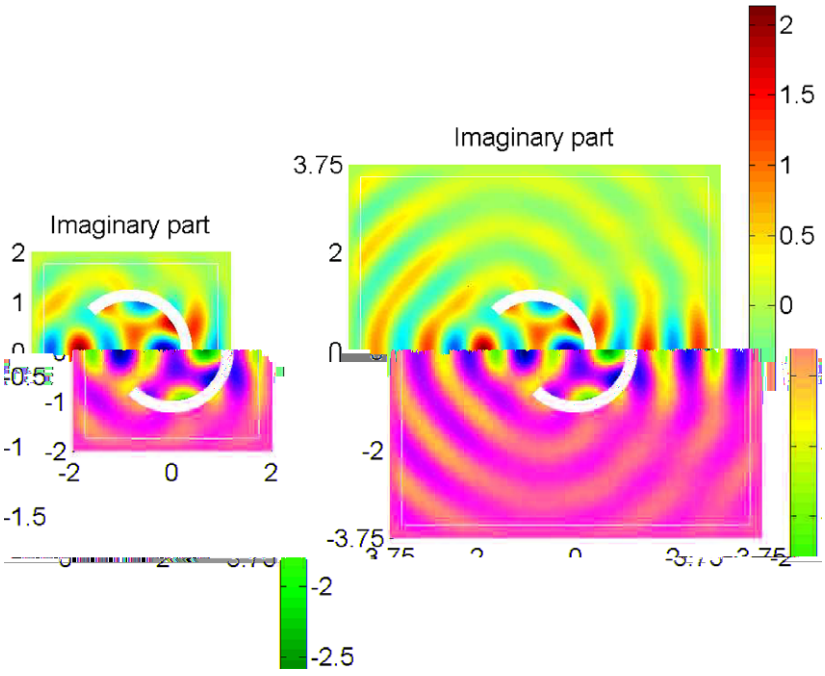

Fig. 21. Reflected wave field generated by an incident plane wave. Imaginary part.

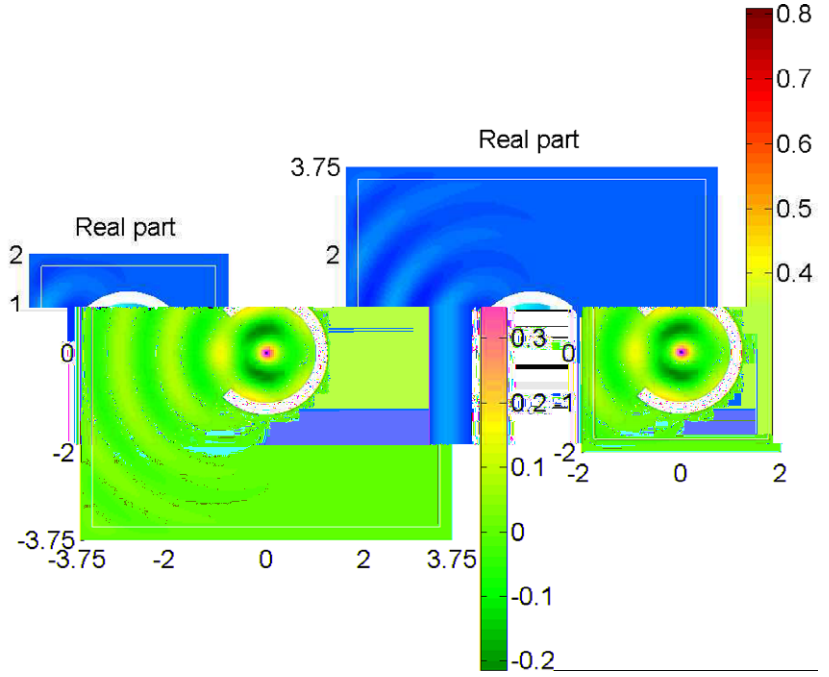

Fig. 22. Wave field generated by a monopole. Real part.

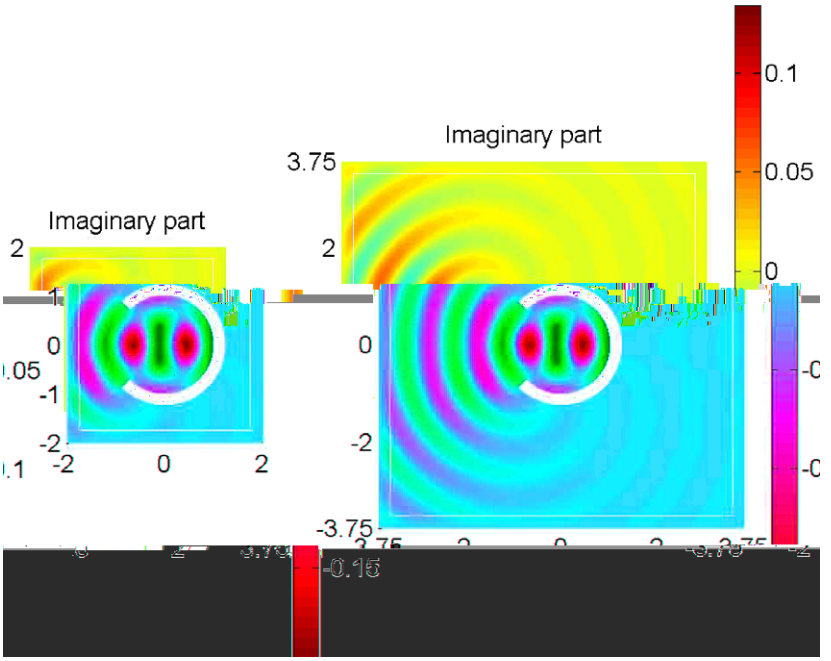

Fig. 23. Wave field generated by a monopole. Imaginary part.

8. Conclusions

We have introduced a PML method based on a non-integrable absorbing function for the numerical solution of time-harmonic problems in unbounded domains. We have shown that this method is able to absorb plane waves with arbitrary incidence angle without any spurious reflection.

We have compared the performance of different non-integrable absorbing functions leading to well posed finite element discretizations. The comparison allow us to choose a particularly simple one, which only depends on the acoustic speed. Therefore, we have obtained a PML method free of unphysical parameters.

We have shown that the proposed method leads to significantly smaller errors than the classical ones based on bounded absorbing functions. To assess the efficiency of our approach, we have applied it to solve some realistic problems, obtaining very good results even with thin absorbing layers close to the obstacles.

As shown in Appendix A, the method is very easy to implement. The integrals in the PML involving the unbounded absorbing function can be computed either explicitly or by means of standard quadrature rules. Let us emphasize that, if quadrature rules are chosen, then there is no need of using hybrid meshes with triangles in the region of interest and rectangles in the PML. A thorough numerical experimentation to validate the proposed PML method on purely triangular meshes will be reported somewhere else.

The method can be readily extended to three-dimensional problems and different coordinates (Cartesian, spherical, etc.). However, many subjects of further research remain open. In particular, a detailed analysis of the proposed PML technique including error estimates for its numerical solution and its application to problems in the time domain.

Acknowledgments

First and third authors were partially funded by MEC (Spain) Research Project DPI2004-05504-C02-02 and Xunta de Galicia Project PGIDIT05PXIC20705PN (Spain). Second author was partially funded by MEC (Spain) Research Projects DPI2004-05504-C02-02 and MTM2004-05796-C02-01. Fourth author was partially supported by FONDAP in Applied Mathematics (Chile).

Appendix A. Computation of the element matrices

Our choice of absorbing functions,

$$\sigma_x(x) = \frac{c}{a^* - x}, \quad \sigma_y(y) = \frac{c}{b^* - y},$$

allows the explicit computation of integrals like those in (4.1). Although such explicit computation is not indispensable, it avoids the use of quadrature rules and their inherent truncation errors.

As an example of explicit computation, consider the integrals (4.2)–(4.4) over an element K as that shown in Fig. 5. In this case, we have to compute four different integrals:

$$\int_{a^*-h_x}^{a^*} \gamma_x(x)(x-a^*)^2\,\mathrm{d}x, \quad \int_{a^*-h_x}^{a^*} \frac{\mathrm{d}x}{\gamma_x(x)}, \quad \int_{b_1}^{b_2} \gamma_y(y)(y-b_j)(y-b_i)\,\mathrm{d}y, \quad \int_{b_1}^{b_2} \frac{\mathrm{d}y}{\gamma_y(y)}.$$

All the integrals that appear in the computation of the element matrices for any other element K in Ω_A are essentially equal to one of these four.

The integrals involving γ_x are computed as follows:

$$\int_{a^*-h_x}^{a^*} \gamma_x(x)(x-a^*)^2\,\mathrm{d}x = \int_{a^*-h_x}^{a^*} \left[1 + \frac{\mathrm{i}}{\omega}\frac{c}{(a^*-x)}\right](x-a^*)^2\,\mathrm{d}x = \frac{h_x^3}{3} - \mathrm{i}\frac{c}{\omega}\frac{h_x^2}{2}$$

and

$$\int_{a^*-h_x}^{a^*} \frac{\mathrm{d}x}{\gamma_x(x)} = \int_{a^*-h_x}^{a^*} \frac{\omega(a^*-x)}{\omega(a^*-x)+\mathrm{i}c}\,\mathrm{d}x = h_x + \frac{\mathrm{i}c}{\omega}\log\left(\frac{\mathrm{i}c}{\omega h_x + \mathrm{i}c}\right).$$

Table A.1
Comparison of quadrature rules using PML with unbounded absorbing functions

ω (rad/s)	Mesh	Gauss–Legendre		Exact integration
		Four nodes	Nine nodes	
250	$N=2$	0.763689	0.770405	0.763485
	$N=4$	0.130572	0.130413	0.130580
	$N=8$	0.028858	0.028755	0.028860
750	$N=2$	1.699869	1.699611	1.699889
	$N=4$	0.446922	0.446910	0.446922
	$N=8$	0.109444	0.109467	0.109443
1250	$N=2$	6.957597	6.958152	6.958012
	$N=4$	1.946417	1.946320	1.946313
	$N=8$	0.429920	0.429913	0.429912

The computation of the integrals involving γ_y depend on the location of the element K. If $-b \leqslant b_1 < b_2 \leqslant b$, then $\gamma_y = 1$ and the integrals are trivial. If $b \leqslant b_1 < b_2 \leqslant b^*$, then

$$\int_{b_1}^{b_2} \frac{\mathrm{d}y}{\gamma_y(y)} = \int_{b_1}^{b_2} \frac{\omega(b^*-y)}{\omega(b^*-y)+\mathrm{i}c}\,\mathrm{d}y = h_y + \frac{\mathrm{i}c}{\omega}\log\left(\frac{\omega(b^*-b_2)+\mathrm{i}c}{\omega(b^*-b_1)+\mathrm{i}c}\right)$$

and

$$\int_{b_1}^{b_2} \gamma_y(y)(y-b_j)(y-b_i)\,\mathrm{d}y = \int_{b_1}^{b_2} (y-b_j)(y-b_i)\,\mathrm{d}y + \mathrm{i}\frac{\omega}{c}\int_{b_1}^{b_2} \frac{(y-b_j)(y-b_i)}{b^*-y}\,\mathrm{d}y.$$

The first integral above is trivial, whereas for the second one straightforward computations lead to

$$\int_{b_1}^{b_2} \frac{(y-b_j)(y-b_i)}{b^*-y}\,\mathrm{d}y = \frac{h_y}{2}(2b^*-b_2-b_1) - h_y(2b^*-b_i-b_j) + (b^*-b_j)(b^*-b_i)\log\left(\frac{b^*-b_1}{b^*-b_2}\right).$$

Similar results are valid if $-b^* \leqslant b_1 < b_2 \leqslant -b$.

Alternatively, all these integrals can be computed using standard quadrature rules. In principle, these rules could lead to large truncation errors due to the singular character of the unbounded absorbing functions. However, our preliminary experiments show that the effect of numerical quadrature does not seem to modify significantly the accuracy of the proposed PML method.

To show this we have solved the numerical test from Section 5 with the integrals computed by Gauss–Legendre rules with four and nine nodes. We report in Table A.1 the relative errors of the solutions computed with each rule and with exact integration.

It can be clearly seen that the errors in the numerical integration are negligible. Moreover, the four-nodes rule shows a slightly better performance, which agrees with the fact that low-order integration schemes are preferable for singular integrands.

References

[1] S. Abarbanel, D. Gottlieb, J.S. Hesthaven, Well-posed perfectly matched layers for advective acoustics, J. Comput. Phys. 154 (1999) 266–283.
[2] R.J. Astley, Infinite elements for wave problems: a review of current formulations and an assessment of accuracy, Int. J. Numer. Methods Eng. 49 (2000) 951–976.
[3] S. Asvadurov, V. Druskin, M.N. Guddati, L. Knizhnerman, On optimal finite-difference approximation of PML, SIAM J. Numer. Anal. 41 (2003) 287–305.
[4] U. Basu, A.K. Chopra, Perfectly matched layers for time-harmonic elastodynamics of unbounded domains: theory and finite-element implementation, Comput. Methods Appl. Mech. Eng. 192 (2003) 1337–1375.
[5] A. Bayliss, E. Turkel, Radiation boundary conditions for wave-like equations, Comm. Pure Appl. Math. 33 (1980) 707–725.
[6] E. Bécache, A.-S. Bonnet-Benn Dhia, G. Legendre, Perfectly matched layer for the convected Helmholtz equation, SIAM J. Numer. Anal. 42 (2004) 409–433.

[7] E. Bécache, P. Joly, On the analysis of Bérenger's perfectly matched layers for Maxwell's equations, M2AN, Math. Model. Numer. Anal. 36 (2002) 87–119.
[8] J.P. Berenger, A perfectly matched layer for the absorption of electromagnetic waves, J. Comput. Phys. 114 (1994) 185–200.
[9] J.P. Berenger, Perfectly matched layer for the FDTD solution of wave–structure interaction problems, IEEE Trans. Antennas Propag. 44 (1996) 110–117.
[10] J.P. Berenger, Three-dimensional perfectly matched layer for the absorption of electromagnetic waves, J. Comput. Phys. 114 (1996) 363–379.
[11] A. Bermúdez, L.M. Hervella-Nieto, A. Prieto, R. Rodríguez, An exact bounded PML for the Helmholtz equation, C.R. Acad. Sci. Paris Ser. I Math. 339 (2004) 803–808.
[12] W.C. Chew, W.H. Weedom, PML 3D perfectly matched medium from modified Maxwell's equations with stretched coordinates, Microwave Opt. Technol. Lett. 7 (1994) 599–604.
[13] F. Collino, P. Monk, The perfectly matched layer in curvilinear coordinates, SIAM J. Sci. Comput. 19 (1998) 2061–2090.
[14] F. Collino, P. Monk, Optimizing the perfectly matched layer, Comput. Methods Appl. Mech. Eng. 164 (1998) 157–171.
[15] F. Collino, C. Tsogka, Application of the PML absorbing layer model to the linear elastodynamic problem in anisotropic heterogeneous media, Geophysics 66 (2001) 294–307.
[16] L. Demkowicz, F. Ihlenburg, Analysis of a coupled finite–infinite element method for exterior Helmholtz problems, Numer. Math. 88 (2001) 43–73.
[17] B. Engquist, A. Majda, Absorbing boundary conditions for the numerical simulation of waves, Math. Comp. 31 (1977) 629–651.
[18] K. Feng, Finite element method and natural boundary reduction, Proceedings of the International Congress of Mathematicians, Warsaw, Poland, 1983, pp. 1439–1453.
[19] D. Givoli, Nonreflecting boundary conditions, J. Comput. Phys. 94 (1991) 1–29.
[20] D. Givoli, B. Neta, High-order non-reflecting boundary scheme for time-dependent waves, J. Comput. Phys. 186 (2004) 24–46.
[21] I. Harari, M. Slavutin, E. Turkel, Analytical and numerical studies of a finite element PML for the Helmholtz equation, J. Comput. Acoust. 8 (2000) 121–137.
[22] T. Hohage, F. Schmidt, L. Zschiedrich, Solving time-harmonic scattering problems based on the pole condition II: convergence of the PML method, SIAM J. Math. Anal. 35 (2003) 547–560.
[23] F.Q. Hu, A stable, perfectly matched layer for linearized Euler equations in unsplit physical variables, J. Comput. Phys. 173 (2001) 455–480.
[24] F. Ihlenburg, Finite Element Analysis of Acoustical Scattering, Springer-Verlag, New York, 1998.
[25] V.J. van Joolen, B. Neta, D. Givoli, High-order Higdon-like boundary conditions for exterior transient problems, Int. J. Numer. Methods. Eng. 63 (2005) 1041–1068.
[26] M. Lassas, E. Somersalo, On the existence and convergence of the solution of PML equations, Computing 60 (1998) 228–241.
[27] J.L. Lions, J. Métral, O. Vacus, Well-posed absorbing layer for hyperbolic problems, Numer. Math. 92 (2002) 535–562.
[28] I.M. Navon, B. Neta, M.Y. Hussaini, A perfectly matched layer approach to the linearized shallow water equations models, Monthly Weather Rev. 132 (2004) 1369–1378.
[29] J.-C. Nédélec, Acoustic and electromagnetic equations. Integral Representations for Harmonic Problems, Springer-Verlag, New York, 2000.
[30] Q. Qi, T.L. Geers, Evaluation of the perfectly matched layer for computational acoustics, J. Comput. Phys. 139 (1998) 166–183.
[31] J.J. Shirron, I. Babuška, A comparison of approximate boundary conditions and infinite element methods for exterior Helmholtz problems, Comput. Methods Appl. Mech. Eng. 164 (1998) 121–139.
[32] B. Sjogreen, N.A. Petersson, Perfectly matched layers for Maxwell's equations in second order formulation, J. Comput. Phys. 209 (2005) 19–46.
[33] E. Turkel, A. Yefet, Absorbing PML boundary layers for wave-like equations, Appl. Numer. Math. 27 (1998) 533–557.
[34] Y.Q. Zeng, J.Q. He, Q.H. Liu, The application of the perfectly matched layer in numerical modeling of wave propagation in poroelastic media, Geophysics 66 (2001) 1258–1266.